Continuous Monitoring of a Soil Aquifer Treatment System's Physico-Chemical Conditions to Optimize Operational Performance

Tuvia Turkeltaub[1], Alex Furman[2], Ron Mannheim[2], Noam Weisbrod[1]

[1]Department of Environmental Hydrology and Microbiology, Zuckerberg Institute for Water Research, The Jacob Blaustein Institutes for Desert Research, Ben-Gurion University of the Negev, Sede Boqer Campus, Midreshet Ben-Gurion, 84990 Israel.

[2]Technion – Israel Institute of Technology, Civil and Environmental Engineering, Haifa 32000, Israel

Correspondence to: Tuvia Turkeltaub (tuviat@bgu.ac.il)

Highlights

- *Long wetting stages reduce soil percolation capabilities during winter.*
- *Redox and gaseous O_2 display intensive dynamics in the top 25 cm of the soil aquifer treatment vadose zone.*
- *Optimal wetting and drying stages are defined according to E_h and gaseous O_2 observations.*
- *The length of wetting and drying stages should be defined separately rather than by adhering to their ratio.*

24   **Abstract**

25   Soil aquifer treatment (SAT) is a tertiary process for wastewater treatment where the wastewater

26   infiltrates through a thick vadose zone for purification and storage in the underneath aquifer.

27   SAT infiltration basins are typically flooded intermittently, while maintaining a fixed ratio

28   between the wetting and the drying stages. However, infiltration basins exhibit different physical

29   and chemical properties, limiting the generalization of SAT operation to attain optimal

30   efficiency. Since frequent sampling of the soil pore water to verify the SAT's biodegradation

31   efficiency can be arduous, continuous monitoring of the SAT vadose zone's physico-chemical

32   conditions is required. In this study, redox potential (E_h) was continuously monitored, together

33   with other variables such as volumetric water content (θ), soil temperature, and gaseous oxygen

34   (O_2), at multiple depths of a SAT vadose zone throughout the year and while the system was

35   constrained to different operational modes. Hydrological models were calibrated and validated to

36   water content observations, and they illustrated the seasonal changes in water infiltration.

37   Furthermore, it was shown that under long wetting stages during winter, there was a reduction in

38   the SAT's drainage capabilities. The E_h observations, under long wetting stages, demonstrated

39   larger variability and very negative values as ambient temperature increased. Assembling the

40   daily E_h observations illustrated that a wetting stage should cease after about 30 hours, once

41   suboxic conditions are established. A drying stage's optimal duration should be 36 hours,

42   according to the E_h and O_2 observations during summer and winter. Ultimately, the study shows

43   that the length of wetting and drying stages should be defined separately, rather than by adhering

44   to the wetting/drying ratio.

45

46

1 Introduction

Worldwide water scarcity has motivated the development of alternative water resources such as the reuse of treated wastewater. Soil aquifer treatment (SAT) is commonly implemented to further improve the recovered water's quality and remove the majority of suspended matter, microorganisms, viruses, and organic and inorganic constituents (Dillon, 2005; Goren et al., 2014; Massmann et al., 2006; Schmidt et al., 2011; Tsangaratos et al., 2017). In SAT systems, the treated wastewater is recharged to the underlying aquifer by surface spreading over infiltration basins. The wastewater is purified mainly through the physical and biochemical processes that occur during water passage through the vadose zone (Dillon, 2005; Elkayam et al., 2015). Although SAT systems have been used for decades (Grinshpan et al., 2021; Bouwer, 2002), the ability to estimate and predict a SAT system's performance is still challenging, and the optimal SAT operation is still under investigation (Ben Moshe et al., 2020; Sharma and Kennedy, 2017).

A major uncertainty in SAT systems concerns the vadose zone processes that play a central role in determining the quality of the water that recharges the aquifer (Elkayam et al., 2015). The chemistry of the percolating wastewater changes due to a combination of several biogeochemical processes, such as organic matter biodegradation, nitrification, sorption, cation exchange, etc. (Amy and Drewes, 2007; Díaz-Cruz and Barceló, 2008; Goren et al., 2014; Miller et al., 2006; Tufenkji et al., 2003). Most of the organic matter is removed by biodegradation (i.e. microbial activity) within the upper two meters of the vadose zone (Drewes, 2009). Nevertheless, the microbial activity is greatly affected by the soil water content, which frequently changes in SAT. Generally, a major challenge in SAT systems is to facilitate the intrusion of O_2, primarily in the gaseous phase, and to enrich the active subsurface with O_2 (Ben Moshe et al., 2020; Massmann et al., 2006).

A consequence of the perturbation in the O_2 supply to SAT is expressed in changes in the redox conditions (Mächler et al., 2013; Rezanezhad et al., 2014). Redox potential or oxidation-reduction potential is a quantitative measure of electron availability, i.e., the tendency of the system to receive or donate electrons (Hinchey and Schaffner, 2005). Substantial changes in SAT systems' redox conditions might lead to the release of undesirable metals, such Fe^{2+} and

76   Mn^{2+} (Goren et al., 2012), and affect the degradation rates of pesticides and pharmaceutical

77   substances (Massmann et al., 2006). Additionally, previous studies have illustrated the possible

78   degradation of groundwater quality due to the emergence of contaminants that leach from the

79   SAT vadose zone under reducing conditions (Asano and Cotruvo, 2004; Massmann et al., 2006;

80   Oren et al., 2007; Sharma and Kennedy, 2017). Redox processes are associated with the

81   degradation of organic matter by terminal electron acceptors or redox couples, such as O_2/H_2O,

82   NO_3/N_2, MnO_2/Mn^{2+}, Fe^{3+}/Fe^{2+}, and SO_4/H_2S, in sequential order from the highest energy yield

83   downwards (Berner, 1981; Froelich et al., 1979; Christensen et al., 2000). The transition between

84   redox conditions is determined by the presence and availability of these electron

85   acceptors/donors. Once the strongest oxidizing species (O_2) is depleted, the next strongest

86   oxidizing species is used (NO_3) and so on. The alternation between oxic (> 400 mV), suboxic

87   (between 400 and -100 mV), and anoxic (-100 mV >) conditions in the vadose zone depends on

88   the availability of the oxidized species (Reedy et al., 2000). In addition, studies have reported on

89   the seasonal (temperature changes) effects on redox conditions, which were attributed to the

90   increase in dissolved oxygen concentrations at low temperatures (Massmann et al., 2006) and the

91   greater microbial activity (i.e., higher O_2 consumption) at higher temperatures (Greskowiak et al.,

92   2006; Kirschbaum, 1995).

93   An important operational aspect of a SAT system is the intermittent application of the effluents

94   (Sattar, 2016; Sallwey et al., 2020). After the infiltration basin is flooded with wastewater, a

95   drying period is implemented to sustain the SAT's infiltration capacity and biochemical

96   capabilities (Sharma and Kennedy, 2017). The wetting and drying stages, which can be

97   expressed by the wet/dry ratio parameter, have a critical impact on the removal rates of dissolved

98   organic carbon, total nitrogen, and pathogens (Ben Moshe et al., 2020; Morrison et al., 2020;

99   Sharma and Kennedy, 2017). Although the wet/dry ratio can vary depending on location and

100 wastewater quality, it is well accepted that it should be below 1.0 (Sattar, 2016; Sharma and

101 Kennedy, 2017). Nevertheless, infiltration basins behave differently with regard to infiltration

102 rates and clogging. Thus, in many cases, the SAT operational efficiency is limited to the personal

103 experience of the operators and their knowledge of the specific infiltration basin (Sharma and

104 Kennedy, 2017). Note, however, that several studies (e.g., Ben Moshe et al., 2021b) suggest that

105 it is not the wet/dry ratio that should be considered, but specific times for wetting and drying.

106 The oxidation-reduction potential (E_h), together with chemical and physical parameters such as
107 water content, soil temperature, O_2 concentration, etc., can be continuously monitored by
108 installing the relevant sensors. Previous studies have implemented the E_h sensor and successfully
109 described, with high temporal resolution, the subsurface chemical conditions in various
110 environments, such as wetlands, the groundwater (or the capillary fringe), aquifers, etc. (Wallace
111 et al., 2019; McMahon and Chapelle, 2008; Shenker et al., 2005; Silver et al., 2018; Rezanezhad
112 et al., 2014). To improve SAT system performances, the link between the wetting and drying
113 stages and the subsequent redox conditions developed in the subsurface should be established.
114 Thus, in situ monitoring can improve SAT management performance and reduce the subjectivity
115 of the operator. The objective of this study was to examine the temporal variability in redox
116 potential and the way it is affected by changes in volumetric water content, gaseous O_2, and
117 climate imposed by different operational modes of wetting and drying stages. Furthermore,
118 calibrated and validated hydrological models were used to explore the behavior of water fluxes
119 under different operational modes and seasonal temperature changes. Finally, the optimal lengths
120 of a drying stage and a wetting stage were determined, following the in situ observations.

121

122 2 Methods

123 Study sites

124 The Dan region reclamation project (Shafdan) reclaims about 125 million m^3 of effluent
125 annually, from the Tel Aviv metropolitan area in Israel. The treatment of effluents occurs in two
126 stages. The first stage involves mechanical-biological treatment, which is based on activated
127 sludge, while in the second stage, the treated water (a secondary effluent) is delivered to
128 infiltration basins, as part of the SAT system, to further improve water quality. Six infiltration
129 basin sites, covering a total area of 1.053 km^2, are located in central Israel, overlying the coastal
130 aquifer (Figure 1). Each basin is divided into several spreading ponds, about 1500 m^2 each,
131 which are alternately flooded. The vadose zone that underlies the basins is mostly composed of
132 sand, sandy loam soil, and calcareous sandstone layers. Typically, the ponds are flooded for one
133 to two days (max hydraulic head of about 50 cm), followed by two to six days of drainage and
134 soil surface drying. The wetting and drying stages are controlled by the ponds' flooding order,

135 the availability of effluent, and the drying period, which is suggested to be at least 24 h (Icekson-

136 Tal et al., 2003). The basin surface is plowed on a regular basis to break up the developed

137 biocrust and to prevent clogging (see Negev et al. (2020) for details).

138 **Study operation**

139 In this research, two in situ measurement stations were installed in an infiltration pond during

140 2018 (pond 4103 in the Yavne 1 cluster, Figure 1). Each station was equipped with several sets

141 of sensors at 25, 50, 75, 100 and 150 cm depth, including time domain transmittance (TDT)

142 probes (Acclima Inc., Idaho, USA), copper-constantan thermocouples (OMEGA Engineering,

143 Inc., Connecticut, USA), oxidation-reduction potential (ORP) electrodes (ELH016 van London

144 Co, Houston, TX, USA), and O_2 percentage probes (ICT02 sensor, ICT Int., Australia). Data

145 were collected at prescribed intervals and logged on a CR1000 data logger (Campbell Scientific,

146 Inc., Logan, UT, USA). In addition, suction cups were installed at similar depths. In station 1

147 (Figure 1), the data consisted of volumetric water content (θ), soil temperature (T), and ORP (E_h)

148 time series, which were continuously measured every 20 minutes between 28/07/2020 and

149 10/02/2021 (total of 14,185 values, 197 days, for each variable). The data were obtained at 25,

150 50, and 100 cm depths. In station 2 (Figure 1), θ, T, gaseous oxygen (O_2), and E_h were measured

151 every 20 minutes between 08/05/2019 and 20/07/2020. There were about 60 days in which data

152 were not collected in station 2 due to technical issues. The data from station 2 contained 27,222

153 points of θ, 29,394 points of O_2, 30,414 points of E_h, and 26,730 points of T measurements. In

154 station 2, the data were collected at 25, 50, 75 and 100 cm depths.

155 The water quality characteristics of the secondary effluent that flooded the Yavne 1 basin are

156 presented in the *Supporting Information* (Fig. S1). Note that the quality parameter concentrations

157 conform to the updated "Inbar" regulations (Inbar, 2007) and the findings of a previous study

158 that surveyed numerous wastewater storage and treatment reservoirs across the country (Kfir et

159 al., 2012). To determine the soil physical properties, undisturbed soil cores were sampled at

160 different depths. Subsequently, flow experiments were carried out to calculate the saturated

161 hydraulic conductivity (*Ks*) based on Darcy's Law (*Supporting Information,* Fig. S2).

162 Additionally, particle size distribution (PSD) analyses are presented in Fig. S3 (*Supporting*

163 *Information*). The PSD results indicate that the SAT vadose zone is homogeneous.

164
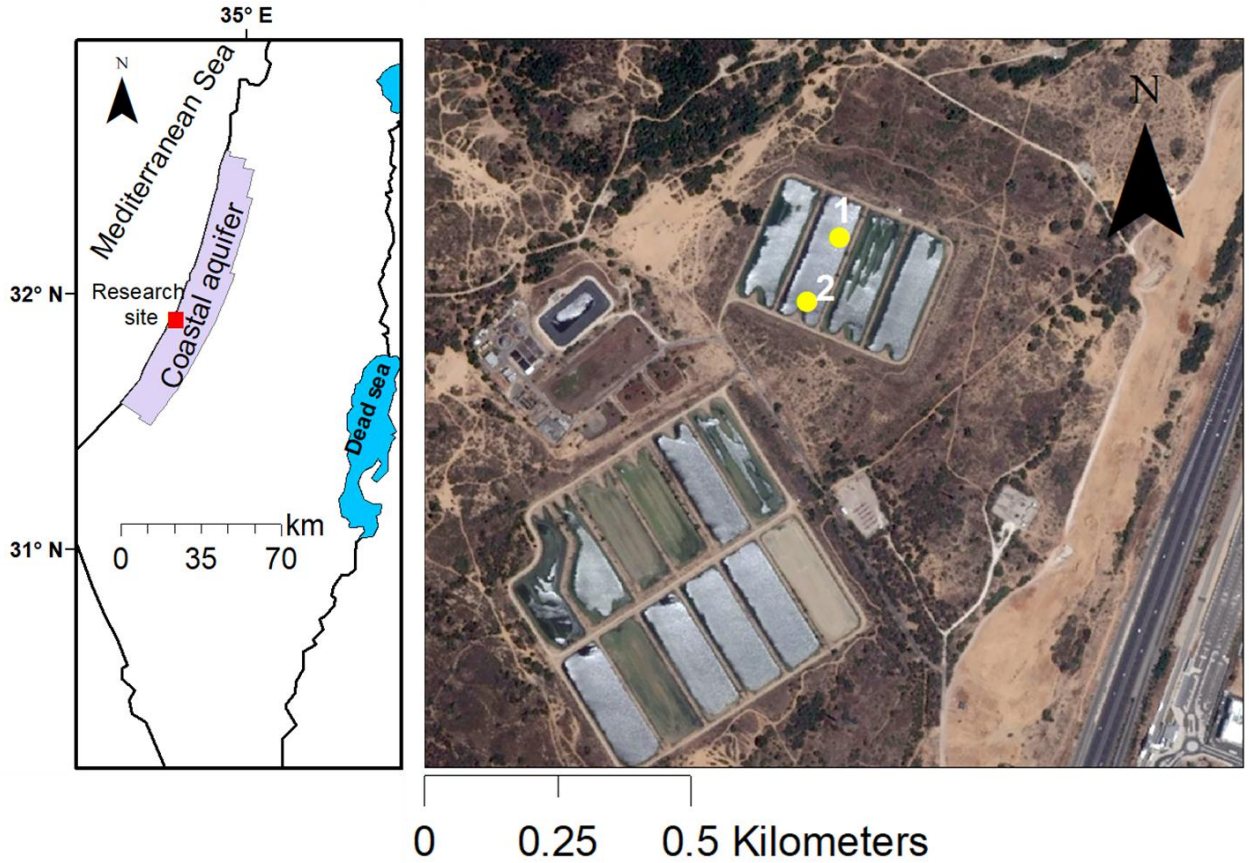
Figure 1: *The location of the investigated site, the Yavne 1 infiltration basin of the Shafdan.*
In the close up of the investigated pond, the yellow circles represent the locations of the
measurement stations (©Google Earth).

Hydrological model and gaseous oxygen dynamics

The calculations for water and oxygen fluxes in the SAT vadose zone are calculated differently
for the ponding stage and for the stage where there is no ponding (water) on the soil surface. For
the ponding stage, Ganot et al. (2017) showed that the infiltration rates in managed aquifer
recharge systems can be predicted reasonably well by simple analytical models. In this study, the
Green-and-Ampt equation for infiltration into a flooded soil was implemented to calculate the
water flux (Bouwer, 2002):

$$q = Ks \times \frac{(L + d - \psi^*)}{L} \quad (1)$$

177   where q (L T^{-1}) is the water flux, d (L) is the ponding depth, L (L) is the thickness of the

178   saturated vadose zone, and ψ^* (L) is the negative pressure head at the wetting front. Note that L

179   is assumed here to be constant, the subsurface is assumed to be homogeneous, and θ is assumed

180   to vary with time only. As the wetting front progresses, the gradient approaches a value of unity,

181   and the infiltration rate becomes equal to the hydraulic conductivity of the wetted zone. Once the

182   water ponding ceases, the water drainage is set equal to the unsaturated hydraulic conductivity,

183   described with an exponential form (Guswa et al., 2002):

184
$$D(\theta) = Ks \frac{e^{\beta(\theta-\theta_{fc})} - 1}{e^{\beta(\theta_s-\theta_{fc})} - 1} \quad (2)$$

185   where Ks (L T^{-1}) is the saturated hydraulic conductivity, β is a parameter of the soil, θ (L^3 L^{-3}) is

186   the volumetric water content, θ_{fc} (L^3 L^{-3}) is the water content at field capacity, and θ_s (L^3 L^{-3}) is

187   the saturated water content. Furthermore, the effect of temperature changes on the soil hydraulic

188   conductivity is implemented through the change in viscosity (Lin et al., 2003):

189
$$Ks_T = Ks_{25} \frac{\mu_{25}}{\mu_T} \quad (3)$$

190   where Ks_T and Ks_{25} are soil hydraulic conductivity values at temperature T$^\circ$C and 25° C,

191   respectively, and μ_T and μ_{25} are the dynamic viscosity of water (M L^{-1} T^{-1}) values at T$^\circ$C and 25°

192   C, respectively.

193   An inverse problem was set to find an optimal combination of Ks and β parameters that

194   minimizes the following objective function:

195
$$\Phi(b) = \sum_{i=1}^{N} [\theta(t_i) - \theta(t_i, b)]^2 \quad (4)$$

196   where N is the number of the θ observations, $\theta(t_i)$ are the observations at a specific time, and

197   $\theta(t_i,b)$ are the corresponding models' (Eq. 1 to 3) predictions for the vector of optimized

198   parameters, b (Ks and β). The inverse problem was solved using the *fminsearch* function in

199   MATLAB. To evaluate the prediction quality, the root mean squared error (RMSE), the Nash

Sutcliffe efficiency (NSE), and the Pearson correlation (r) were calculated following Ritter & Muñoz-Carpena (2013).

3 Results and Discussion

The water level measurements at the soil surface were collected by the Shafdan operators as part of the operational routine. Analysis of the water level data (ponding depth) indicates two operational modes of long and short cycles that were implemented at the investigated pond. The characteristics of the drying and wetting stages, as recorded by the operators, are summarized in Table 1. Note that the wetting stage is defined when water is present at the soil surface and the drying stage is defined when water is absent. Further note that the water level is measured at a single point (close to the pond inlet). Therefore, some variations, at the order of a few cm, may exist due to microtopography and the distance between the inlet and the far parts of the pond. This may lead to some delays in water arrival or recession from the stations. Throughout the analysis described below, we define the winter period as the months between November and April and the summer period as the months between May and October, corresponding to the Mediterranean climate. Our monitoring systems are operated independently from the Shafdan facilities.

Table 1. Technical information of the recorded long and short wetting and drying cycles (this data was provided by the Shafdan operators).

	Long cycles	Short cycles
Wetting stage (days)	9 ± 2.4	1.5 ± 0.4
Drying stage (days)	3.3 ± 2.4	1.8 ± 1
Number of recorded cycles	33	37
Length of cycle (days)	12.7 ± 3	3.2 ± 1.3
Wet/dry ratio	3 ± 1.8	0.9 ± 0.3

Hydrological conditions

222   A representative set of θ time series measured in the SAT's vadose zone is presented to describe

223   the variability in hydrological conditions measured throughout different seasons and operational

224   modes (Figure 2). The θ measurements were obtained during long (Figure 2a, b, c) and short

225   (Figure 2d) cycles at three different depths. Note that the water content measurements presented

226   in Figure 2 (a, b) were recorded at station 2 (Figure 1), during summer (Figure 2a) and winter

227   (Figure 2b). The water content variations under short cycles were measured at station 1 (Figure

228   2c, d). Differences in the absolute values between the water content observations at different

229   depths are mainly related to the vertical texture variability (Fig. S2, *Supporting Information*).

230   Under the long cycles, θ measurements were obtained throughout 19 cycles during summer

231   (May–October) and 14 cycles during winter (November–April). Under short cycles, there were

232   12 cycles during summer and 25 during winter.

233   Every recorded wetting event prompted an intensive infiltration that was expressed by a rapid

234   and almost instantaneous increase in water content at all depths and under the two operational

235   modes (Figure 2). Furthermore, the soil remained at similar level of saturation throughout each

236   wetting stage. Similarly, once the drying process started, it occurred virtually simultaneously at

237   all depths. There were noticeable differences in the drainage rates between summer and winter,

238   where the soil dried faster in summer. To elaborate the drainage process, the drying stages were

239   assembled and averaged at an hourly interval and separated into short (Figure 3a) and long

240   (Figure 3b) cycles. Additionally, Eq. (1), (2), and (3) (the hydrological model) were implemented

241   to describe the water flow in the SAT's vadose zone under long and short cycles. The

242   hydrological models were calibrated and validated against water content observations at 25 cm

243   depth by adjusting the Ks and β parameters (Fig. S4 and Fig. S5, *Supporting Information,* Table

244   2). Throughout the calibration, the Ks and β parameters attained different values for the long

245   cycle periods and the short cycle periods (Table 2). There are differences in soil physical

246   properties between stations 1 and 2, which explains the need for calibrating different parameter

247   sets. In addition, the calibrated Ks values for both models were substantially lower than the

248   measured Ks values (Fig. S2, *Supporting Information,* Table 2). It has been shown that Ks

249   measurements in the field are commonly lower than lab Ks measurements (Nimmo et al., 2009).

250   This is related to a reduction in soil conductivity due to air trapping in the soil pores during the

251   wetting process when water is applied at the land surface (Mizrahi et al., 2016; Nimmo et al.,

252   2009).

253   Under the short cycles, the soil drainage process occurred mostly within the first 15 hours of the

254   drying stage (Figure 3a). The soil drainage rate was slightly higher in summer than in winter.

255   Under the short cycles, the model successfully followed the observed trends, where the

256   validation period showed similar performances (Fig. S4 and Figure 3a). The model results for the

257   short cycles confirm that the differences in drainage between summer and winter are mainly due

258   to temperature changes that affect water viscosity (Lin et al., 2003). During the long cycle

259   application, the drainage rates in summer showed a moderate θ decline compared to the observed

260   θ under short cycles (Figure 3b). This might be due to the differences in soil physical parameters

261   between stations 1 and 2, as highlighted by the calibrated models' parameters (Table 2).

262   While the model under long cycles successfully followed the drainage trend during summer, the

263   model showed poor performance during winter under long cycles. This is mainly due to the

264   observable changes in θ measurements, which displayed a shift towards higher values from

265   November 2019 (Fig. S5 and Figure 2b). To explore the changes in the SAT's physical

266   properties, an additional parameter set was calibrated against the winter data only during the long

267   cycles (Figure 3b, green line). Both the Ks and β parameters attained lower values, and the θ_s

268   increased (Fig. S6 and Table 2). Previous studies related the accumulation of organic matter in

269   SAT to lower rates of organic matter decomposition during winter (Nadav et al., 2012a, b; Arye

270   et al., 2011). The authors ruled out the occurrence of soil clogging and indicated that the

271   accumulation of organic matter at the topsoil increased the degree of soil water repellency or soil

272   hydrophobicity. This phenomenon often develops in sandy soils (commonly used in SAT) due to

273   the low specific surface area of sand (~0.0077 g m^{-2}) compared to clay (~900 g m^{-2}) (Doerr et al.,

274   2000; Wallis and Horne, 1992). Thus, only a small amount of organic matter is required to coat

275   the particles of the sand in order to develop soil water repellency (Wallis and Horne, 1992). Arye

276   et al. (2011) showed that soil hydrophobicity is attributed to the reduction of liquid surface

277   tension and increase of the contact angle. These changes in soil properties are related to the

278   reduction of the soil permeability (Nadav et al., 2012b). It appears that long wetting and drying

279   cycles in SAT during winter can alter the physical soil properties, which eventually affect the

280   infiltration capabilities.

281

282

283
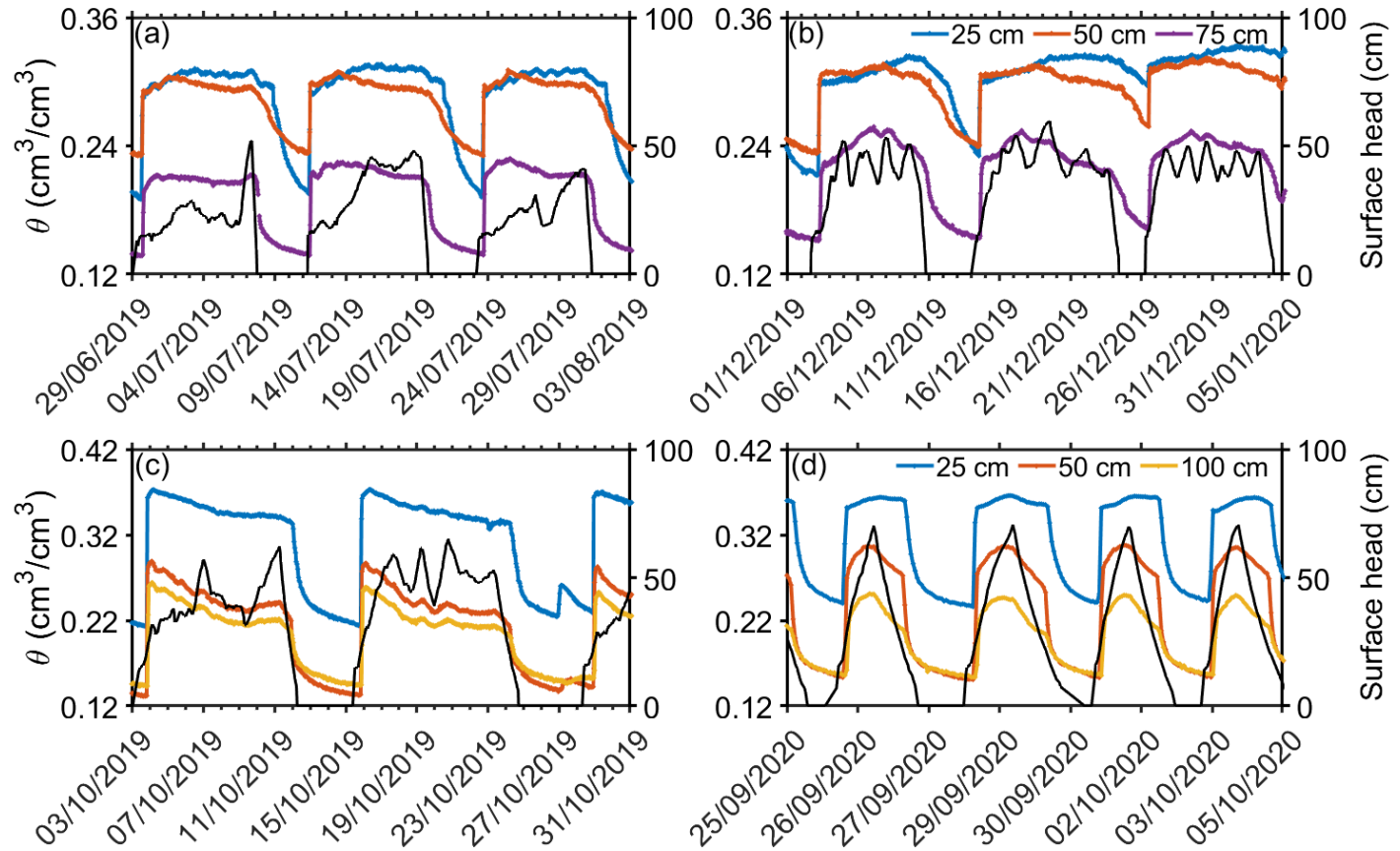
Figure 2: *Representative time series of θ measurements obtained at station 2 (Figure 1) during (a) summer*
and (b) winter under long wetting and drying cycles at three different depths. Black line represents the
surface water hydraulic head. The bottom plots display θ measurements obtained at station 1 under (c)
long and (d) short wetting and drying cycles during the summer.

Table 2. Estimated parameters of the hydrological models

	Station 1	Station 2	Station 2 (winter only)
Ks **(cm h^{-1})**	**5**	**0.9**	**0.72**
θ_s	0.36	0.32	**0.33**
β	**30**	**6.75**	**6.48**
θ_{fc}	0.19	0.19	0.19
ψ^* **(cm)**	-15	-15	-15

θ_h	0.05	0.05	0.05

290

291
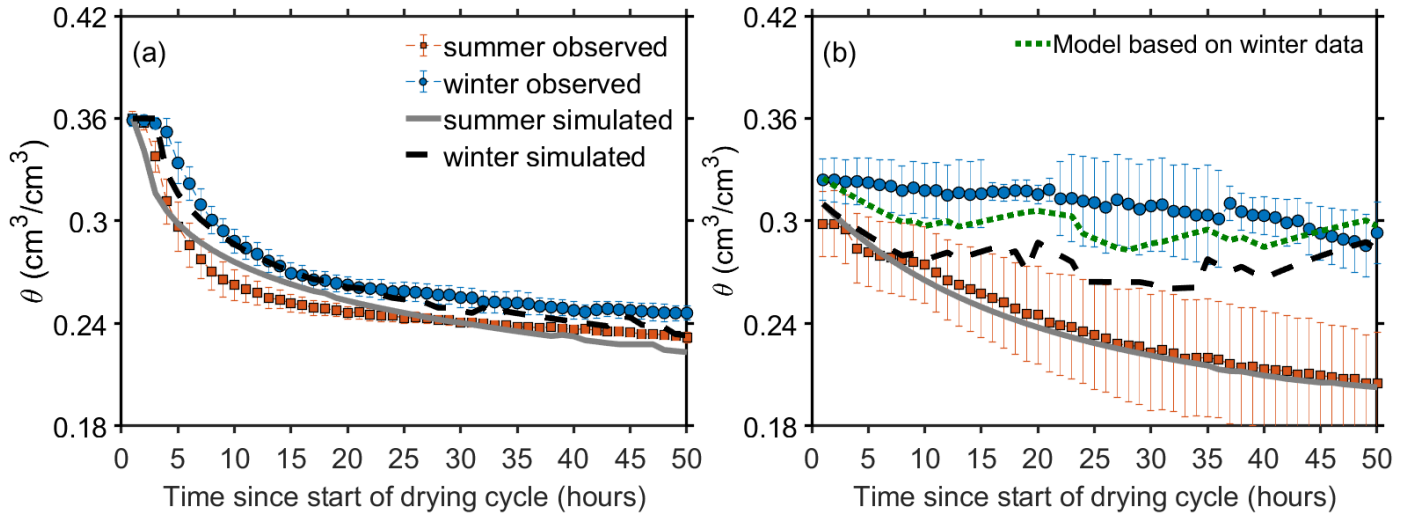
Figure 3: *The average and standard deviation values of measured θ at 25 cm depth throughout the drying stages at an hourly time scale: (a) short cycles (station 1) and (b) long cycles (station 2). The blue and red circles represent the average θ values collected during winter (November– April) and summer (May–October), respectively. The statistics of measured θ under long cycles are based on 19 drying stages during summer and 14 drying stages during winter. For the short cycles, the statistics are based on 12 drying stages during summer and 24 drying stages during winter. The dashed black and solid gray lines represent the average values of simulated θ throughout the drying stage during winter (November–April) and summer (May–October), respectively. Note that for the long cycle periods, an additional model was established based only on winter data (green line).*

292
293
294
295
296
297
298
299
300
301

302

Seasonal differences in SAT redox (E$_h$) conditions under long wetting cycles

E$_h$ conditions were monitored at four depths (Figure 4a, b). The behavior of the E$_h$ dynamic following a wetting event was similar for the summer and the winter periods. At 25, 50, and 75 cm depths, a gradual decline in E$_h$ started only after a time lag from the beginning of a wetting event (Figure 4a, b). This time lag can be explained by the presence of dissolved oxygen (DO) in the percolating solution. Once DO is depleted, suboxic and anoxic conditions begin to develop

309   (Dutta et al., 2015; Ben Moshe et al., 2021, 2020). The E_h conditions at 25 cm were the most

310   highly responsive to the wetting events, while the E_h conditions were the most negative at this

311   depth (Figure 4a, b). At 100 cm depth, only minor changes were observed, and in some cases

312   (during winter), no changes were observed (Figure 4a, b). According to the gaseous O_2

313   measurements (Figure 4c, d), there were partially aerated conditions (unsaturated conditions)

314   during some of the flooding events at 75 cm depth, while at 150 cm depth, unsaturated

315   conditions prevailed continuously throughout the period of measurements. Therefore, the small

316   changes of E_h at 100 cm depth could either have been the outcome of only minor biochemical

317   activity, or they could have been due to the sufficient oxygen supply. Gorski et al. (2019)

318   suggested that in coarse-grained soils, due to the high infiltration rates, the DO is delivered

319   rapidly by the percolating water to the base of the saturated zone. Thus, the soil microbes do not

320   have enough time to consume the DO. In the current study it is reflected by positive E_h values at

321   100 cm depth (Figure 4a,b). As the wetting cycle continues, the E_h conditions at 100 cm depth

322   decrease, mainly during summer (Figure 4a,b). This indicates that eventually the infiltrated water

323   that reaches 100 cm depth contains lower concentrations of DO. Yet, the E_h conditions do not

324   show further decrease, which can be attributed to limited microbial activity. Previous studies

325   showed that carbon availability at greater depths of the vadose zone is a dominant factor for this

326   limitation (Grau-martínez et al., 2018, 2017; Brettar et al., 2002). Furthermore, the monitored E_h

327   conditions illustrate that most of the activity in SAT systems occurs at the topsoil, as illustrated

328   in previous studies (e.g., Quanrud et al., 1996, 2003; Sopilniak et al., 2017; Grinshpan et al.,

329   2022). Note that the E_h recovery time, i.e., an increase towards positive values, was virtually

330   instantaneous once the drying process initiated (Figure 4a, b). The increase in E_h conditions

331   occurred concurrently with the observed rapid increase of the gaseous oxygen (O_2) in the vadose

332   zone (Figure 4c, d).

333   A distinct difference in E_h conditions between winter and summer at 25 cm depth is expressed by

334   a more negative range of values during summer (Figure 4a, b). Since similar wastewater quality

335   and hydraulic loads were fed to the pond during summer and winter (*Supporting Information*),

336   the E_h conditions were mainly affected by the SAT's aeration state and seasonal temperature

337   changes. In Figure 5, the monthly E_h conditions at 25 cm depth are presented in the form of a

338   boxplot, together with the monthly average ambient temperature (dashed black line) and monthly

339   average global radiation (gray line). The E_h conditions showed a wider range of values with the

340   increase in temperature (Figure 5). Between November and March, the E_h conditions mostly

341   remained above zero or were slightly negative (Figure 5). Once the temperature increased above

342   24°C between May and October, E_h conditions showed substantial fluctuation between negative

343   and positive values (Figure 5). Note that the average monthly ambient temperatures during

344   November and May were similar in value, but during November, the E_h conditions mostly

345   remained above zero (Figure 5). This difference is connected to the daylight duration, as

346   indicated by the global radiation, which is substantially greater in May than in November (Figure

347   5, gray line). A typical characteristic of aquatic systems is the large fluctuations in dissolved

348   oxygen (DO) concentrations due to intense photosynthesis and respiration (Stumm and Morgan,

349   1996). Goren et al. (2014) illustrated that following the effluent spreading in the infiltration

350   ponds, photosynthesis enriches the water with DO. Furthermore, chemical analysis of porewater

351   samples that were obtained at 0.5 m depth in the SAT vadose zone indicated DO's substantial

352   influence on the biochemical conditions of the percolating water (Goren et al., 2014). Thus, the

353   photosynthesis process enriches the effluent with DO, which encourages further microbial

354   activity (Goren et al., 2014; Hargreaves, 2006; Rodríguez-Escales et al., 2020). However,

355   between July and September, there was a decrease in global radiation that did not affect the E_h

356   variability (Figure 5). Thus, it appears that under long wetting stages, the seasonal temperature

357   changes dominate the E_h conditions but show some trade-off with the global radiation.

358
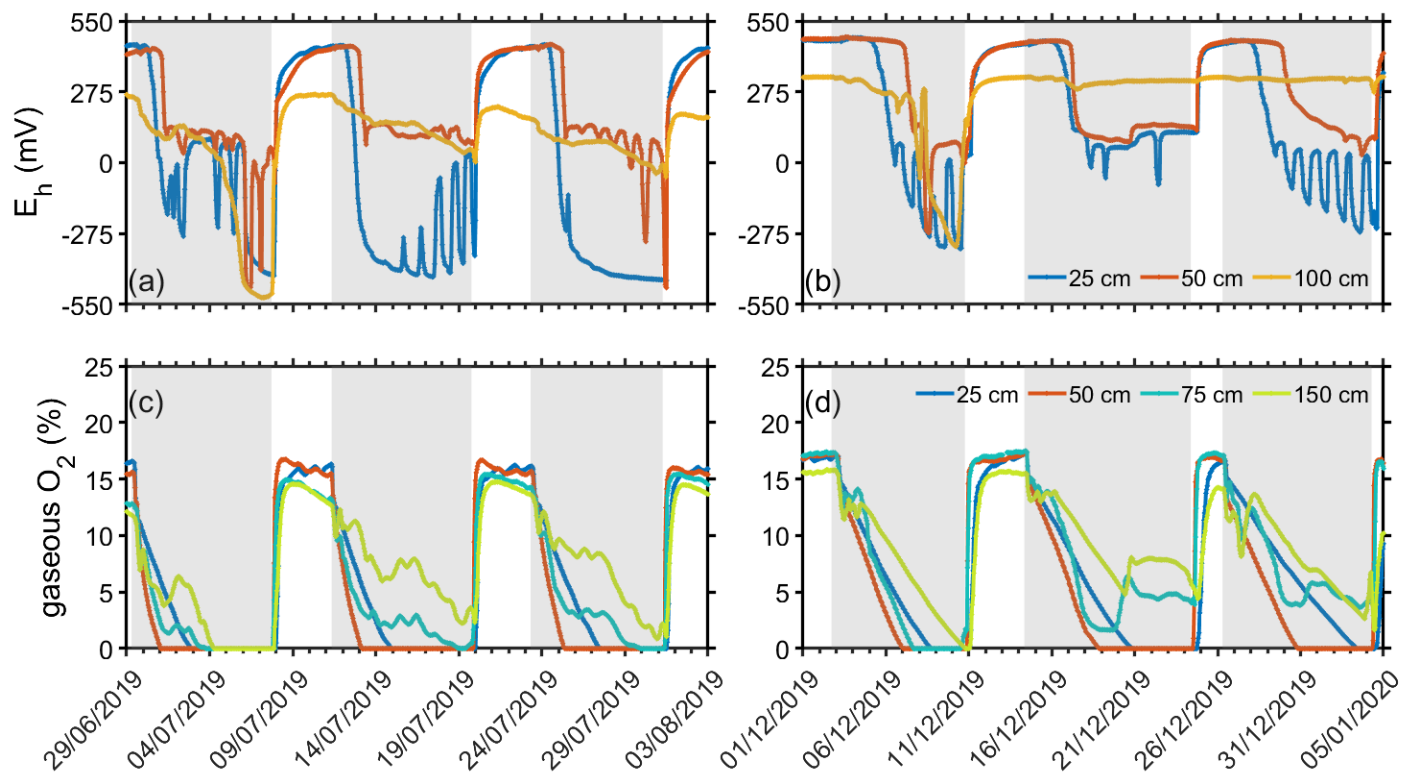
Figure 4: *Representative time series of redox-potential (E_h) and gaseous O_2 measurements*

obtained at station 2 (Figure 1) at depths of 25, 50, and 100 cm: (a, c) summer and (b, d) winter.

Note that the gray and white areas indicate wetting and drying periods, respectively.

362
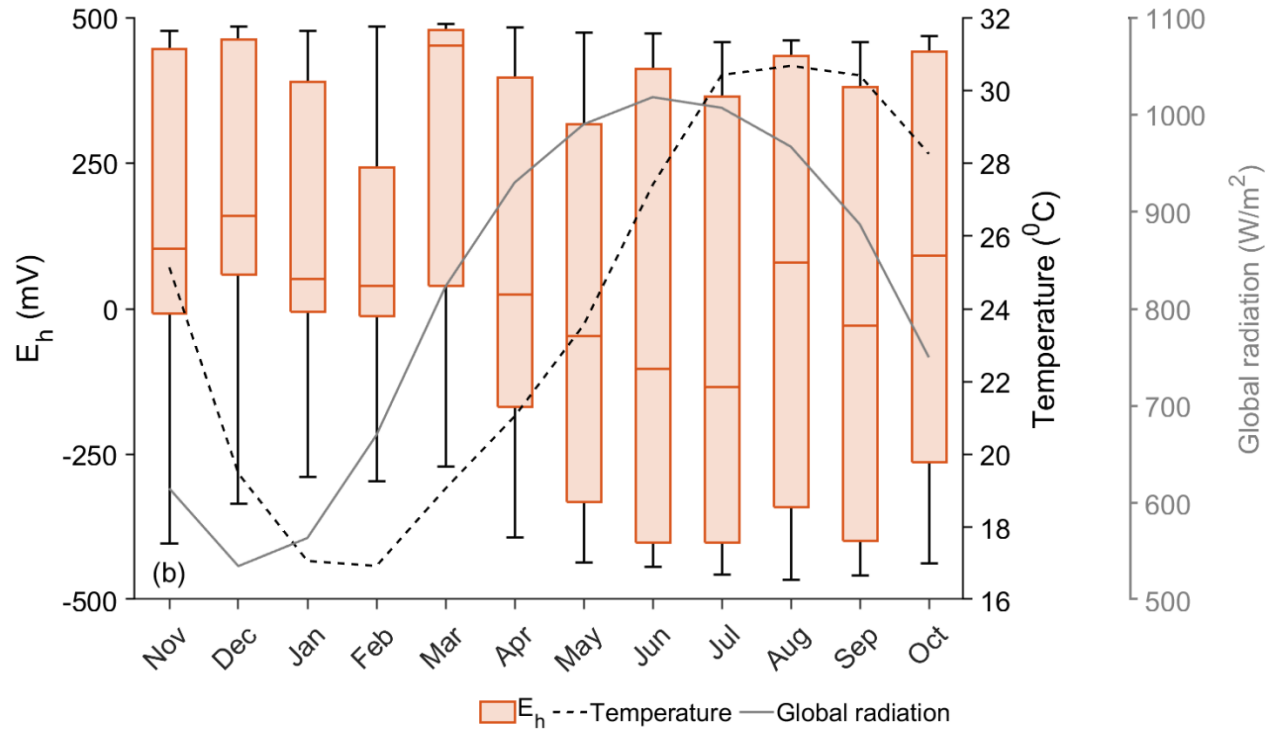
Figure 5: *Seasonal changes in E_h conditions as were observed at 25 cm depth at station 2 under long (seven days) wetting periods. The dashed black line represents the monthly mean ambient temperature, and the solid gray line represents the monthly mean global radiation obtained from the Israeli Meteorological Service (IMS, 2021).*

A comparison between SAT redox (E_h) conditions under long and short cycles

It has been shown that the operational mode affects the aeration conditions of the upper vadose zone, which consequently might alter the infiltration rates and the intensity of the biogeochemical processes (Goren et al., 2014). Throughout the measurement period, the intervals of wetting and drying stages were modified (Table 1). The wetting and drying stages were substantially shortened during September 2020, which enabled examining the differences in E_h conditions under short and long cycles. The variations in E_h conditions under long cycles during October 2019, December 2019, and January 2020 are presented in Figure 6a, c. In addition, the changes in E_h conditions under short cycles during September–October 2020, December 2020, and January 2021 are presented in Figure 6b, d.

379   As was shown above, under long cycles, the E_h conditions declined towards slightly negative

380   values during winter and attained markedly negative values during the summer months at 25 and

381   50 cm depths, where only minor variations were observed at 100 cm depth (Figure 6a, c). The E_h

382   conditions, under short cycles during the summer, showed a decline towards slightly negative

383   values for a brief time compared to long cycles (Figure 6a, b). During the winter, only minor

384   variations in E_h conditions were recorded under short cycles (Figure 6d). Note that at 100 cm

385   depth, there was almost no change in E_h conditions for either season under short cycles (Figure

386   6b, d). As was illustrated previously (Figure 4a, b), once the drying stage initiated, the recovery

387   of E_h towards positive values (oxic conditions) was almost instant under both short and long

388   cycles. It appears that the re-establishment of oxic conditions occurs independently of the length

389   of the wetting stage.

390   The observations of E_h and gaseous O_2 under long and short cycles indicate a weak relationship

391   between the wetting and the drying stages. These results call into question the advantage of

392   implementing the wet/dry ratio for optimizing SAT performance. It appears that the length of a

393   wetting stage and a drying stage should be defined separately (Ben Moshe et al., 2020, 2021).

394   Thus, the necessary further investigation is described below to examine the optimal lengths of

395   the wetting and drying stages.

396

397
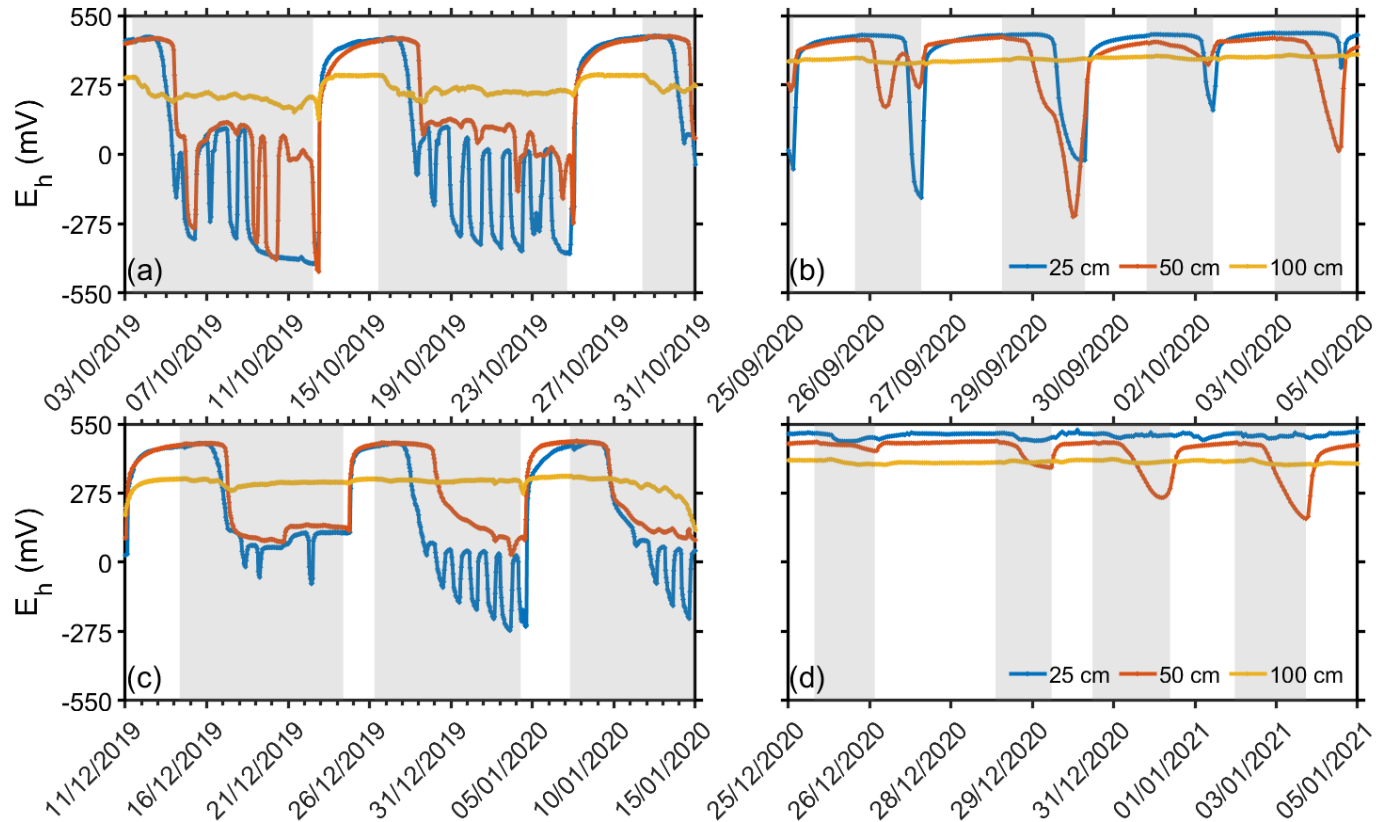
Figure 6: *Representative time series of redox-potential (E_h) measurements at 25, 50 and 100 cm depths in station 1 (Figure 1): (a, c) long wetting periods and (b, d) short wetting periods. Note that the gray and white areas indicate wetting and drying periods, respectively.*

401

The length of the wetting stage according to E_h measurements

During wetting stages, the main limiting factor of the biodegradation process is the availability of dissolved oxygen (Skopp et al., 1990; Cook and Knight, 2003). Once the soil pores are fully saturated, only the dissolved oxygen (DO) of the percolating water is available. However, studies have illustrated that the DO of the percolating water rapidly depletes (Dutta et al., 2015; Ben Moshe et al., 2021, 2020). Thus, the wetting stage should cease when the DO no longer has an effect on the degradation process, i.e., when suboxic and anoxic conditions begin to develop. E_h measurements can provide a good indication for the time when such conditions begin to be established. For this purpose, the hourly measured E_h conditions during the wetting stage of 33 recorded cycles (19 cycles during summer and 14 cycles during winter) were averaged for 25,

412   50, 75 and 100 cm depth (Figure 7). The data were separated between winter (November–April)

413   and summer (May–October), according to the trends presented in Figure 5.

414   During summer, the decline in E_h conditions were steeper compared to the trends exhibited in

415   winter (Figure 7). Following 30 hours of wetting, the E_h conditions during the summer dropped

416   below 400 mV at 25 cm depth, which indicates the establishment of suboxic conditions (Figure

417   7a). After 37 hours, the E_h observations at 50 and 75 cm depths showed similar trends (Figure

418   7a). Note that after 45 hours the E_h observations at 25 cm depth reach anoxic conditions. The

419   differences between E_h measurements at topsoil and at deeper parts of the vadose zone were

420   previously attributed to carbon availability, which decrease with depth (Brettar et al., 2002;

421   Bohrerova et al., 2004). Furthermore, Brettar et al. (2002) provided a range of threshold E_h

422   values for denitrifying conditions depending on the depth of the soil horizon. Similarly, despite

423   the differences between the E_h measurements at 25 cm depth and at deeper depths (Figure 7), all

424   the E_h measurements potentially indicate similar activity. To prevent anoxic conditions in the

425   SAT vadose zone during summer, the optimal length of a wetting stage, in terms of

426   biodegradation, would be about 30 hours (1.25 days). This is in agreement with Dutta et al.

427   (2015), who suggested a relatively wide distribution of de-oxygenation times, between 0.36 and

428   1.5 days.

429   In winter, the E_h measurements decrease towards suboxic conditions, that occur after 51, 69 and

430   84 hours of wetting at 25, 50 and 75 cm depths, respectively (Figure 7b). The delay in E_h drop

431   (compared to summer) is partly explained by the longer presence of gaseous O_2 in the SAT

432   vadose zone (Figure 4c,d and Figure 8). It takes a longer time for the gaseous O_2 to deplete

433   during winter (Figure 8), probably as a result of lower oxygen demand due to slower microbial

434   activity at low temperatures (Kirschbaum, 1995). An additional explanation for the longer

435   presence of gaseous O_2 is due to longer establishment of saturated conditions as a consequence of

436   lower Ks values (see section *Hydrological conditions*). However, once the gaseous O_2 is absent

437   from the SAT vadose zone during winter (Figure 8), no further decrease in E_h conditions occur

438   (Figure 7b). Therefore, the trade-off between nutrient transport rates and reaction rates should be

439   considered, where the supply of the percolated effluent's substrate might be faster than the

440   SAT's degradation capability (Greskowiak et al., 2006). Determining the length of a wetting

441   stage during winter, using solely the E_h and gaseous O_2 measurements, may be challenging.

442   Nevertheless, the changes in soil physical parameters and the seasonal differences in E_h values

443   imply low biodegradation rates during winter. From a practical perspective, the observed E_h

444   values at 25 cm depth during winter are compared with the E_h measurements during summer.

445   Using a two-sample t-test show that the differences in the first 28 hours of a wetting cycle are

446   insignificant. It suggests that the length of a wetting stage during winter should be no more than

447   30 hours, as in the summer period. Nevertheless, given the evidences that are reflected in the

448   measurements of the current study and conclusions from previous studies, the implementation of

449   SAT during winter is questionable. It might be necessary to store the effluents in reservoirs

450   during winter and apply the SAT during summer.

451   According to the E_h sensor at 100 cm, suboxic conditions prevail for most times during winter

452   and a moderate decrease (compared to the other sensors) in E_h conditions is noticeable during

453   summer (Figure 7). The gaseous O_2 observations at 75 cm indicate depletion of gaseous O_2

454   during summer and a very low O_2 concentration (2%) during winter (Figure 8c). At 150 cm, the

455   gaseous O_2 observations suggest that for most of the recorded wetting cycles, unsaturated

456   conditions prevailed (Figure 8d). It is not clear if the E_h conditions at 100 cm are determined by a

457   continuous supply of oxygen given the unsaturated conditions. This might affect the decision

458   concerning the optimal length of a wetting cycle. However, previous studies (Miller et al., 2006;

459   Fox et al., 2005; Lin et al., 2008; Goren et al., 2014; Sopilniak et al., 2018; Essandoh et al., 2013;

460   Quanrud et al., 1996, 2003) and a recent study by our group (Grinshpan et al., 2022) suggest that

461   most biodegradation activity occurs at topsoil and there is a steep reduction in removal

462   capabilities with depth. Thus, the potential contribution of the deeper vadose zone to the SAT

463   treatment should be further investigated.

464

465
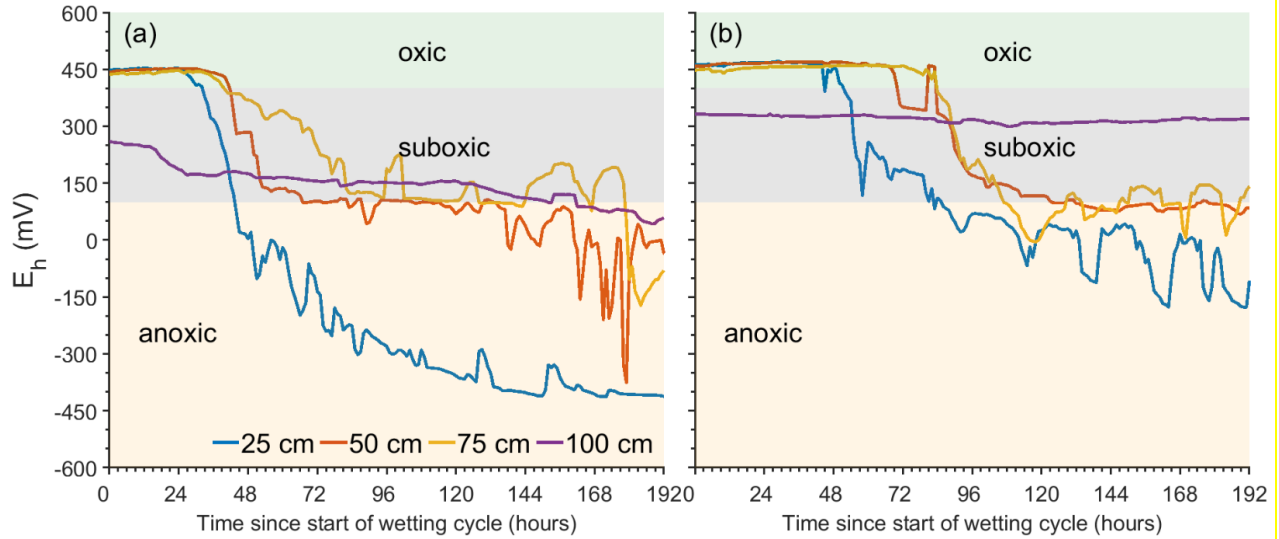
Figure 7: *Plot of hourly means of E_h measurements obtained at station 2, from the beginning of the wetting stages at three depths. The statistics are based on 19 cycles during summer (May–October) and 14 cycles during winter (November–April) that were observed at (a) winter and (b) summer. Note that the data are separated between summer and winter according to the trends presented in* Figure 5. *The green, grey, and yellow areas represent the oxic (400mV <), suboxic (400mV > E_h > 100mV), and anoxic E_h < 100mV) conditions, respectively.*

472

473
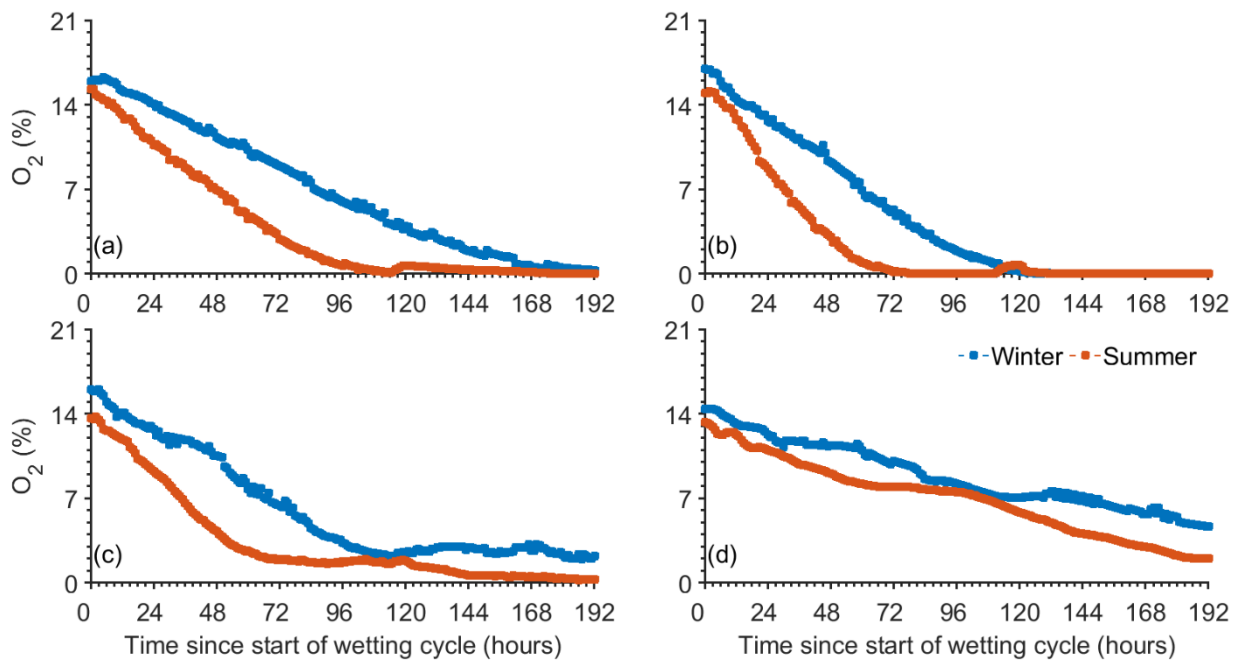
Figure 8. *Plot of hourly means of gaseous O_2 measurements from the beginning of the wetting stages at (a) 25, (b) 50, (c) 75 and (d) 150 cm depths. The statistics are based on 14 cycles during winter (November–April) and 19 cycles during summer (May–October) that were observed at multiple depths in station 2. Note that the data are separated between summer and winter according to the trends presented in* Figure 5.

The length of the drying stage using E_h and gaseous O_2 measurements

The drying stage in SAT systems is implemented to restore the infiltration, biological, and chemical capabilities of the pond, mainly by aerating the soil (Sharma and Kennedy, 2017). A drying stage is defined as the stage in which there is no water at the soil surface, and the observed volumetric water contents begin to decrease (Figure 2). To determine the optimal time for a drying stage, both the averaged values of the E_h (Figure 9a,b) and gaseous O_2 (Figure 9c,d) observations during the drying stages are presented. Note that the E_h measurements were conducted at 25, 50, 75 and 100 cm depths and the O_2 observations were obtained at 25, 50, 75 and 150 cm depths (Figure 9). The E_h and O_2 data during the drying stages were separated between winter (November–April) and summer (May–October), according to the trends presented in Figure 5.

Slower aeration rates and larger variability were observed during winter compared to summer (Figure 9a,b). Furthermore, the E_h recovery is clearly dominated by the rates of the gaseous O_2 intrusion to the soil (Figure 9c,d). During winter, the aeration rates are different at each depth, but in general the gaseous O_2 concentrations increase moderately with time (Figure 9a). The recovery of the E_h conditions display comparable trends (Figure 9c). Although the O_2 sensor at 50 cm depth suggest a faster O_2 intrusion rate compared to the other sensors (Figure 9a), it is not expressed in the E_h recovery time (Figure 9c). During summer all the observed O_2 curves show steep recovery that ceases after about 20 hours (Figure 9b). According to the O_2 observations, the gaseous O_2 intrusion process at 50 and 75 cm depths starts at the very beginning of the drying stage, while at 25 and 100 cm depths there is a two-hour delay (Figure 9b). Nevertheless, the E_h conditions recovery is comparable at all depths (Figure 9d).

502 The E_h observations illustrate that the re-establishment of oxic conditions in the SAT vadose

503 zone is similar during winter and summer (Figure 9c,d). Once the drying stage started, it required

504 about 36 hours for the E_h conditions to reach values in the range of oxic conditions, regardless of

505 the initial value of the E_h conditions (Figure 9c,d). However, a recent study has indicated that

506 using solely the gaseous O_2 concentration to quantify soil aeration status might be inaccurate for

507 some conditions (Ben-Noah et al., 2021). Instead, the authors suggested using the Damkholer

508 number, which is the ratio between characteristic diffusion (i.e., oxygen supply) and soil

509 respiration times. A small Damkholer number would indicate that the O_2 consumption rate is

510 lower than the O_2 supply. Thus, although during summer the oxygen supply rate is relatively

511 high compared to winter (**Error! Reference source not found.**a,b), the oxygen consumption

512 rate for soil respiration is expected to be substantially higher during summer than during winter

513 (Kirschbaum, 1995), as it is reflected by the E_h observations (Figure 5 and Figure 7). Therefore,

514 in parallel to proper treatment of aeration time, optimal wetting time should be further treated.

515

516
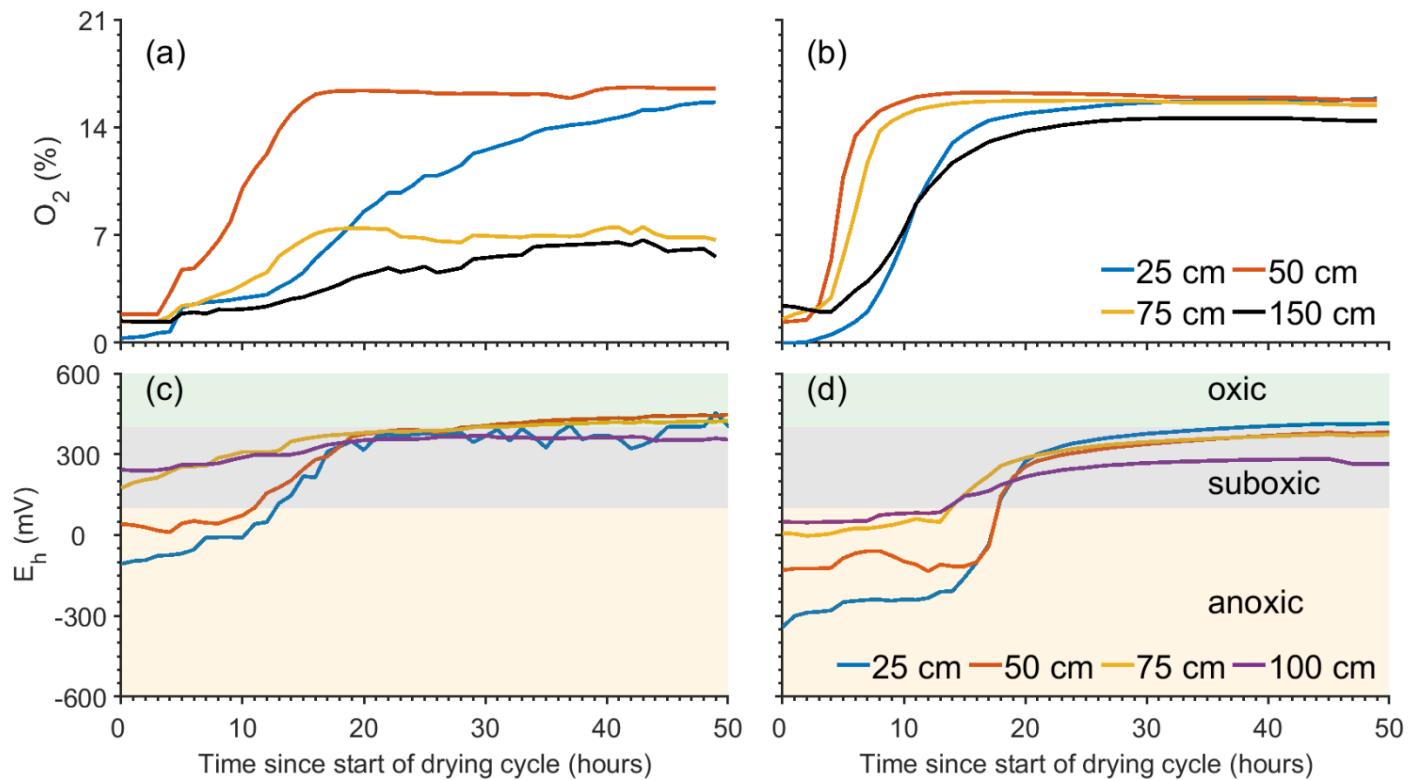
517

518   Figure 9: *Plot of hourly means of E_h and gaseous O_2 measurements from the beginning of the drying*

519   *stages. The statistics are based on (a,c) 14 cycles during winter (November–April) and (b,d) 19 cycles*

520   *during summer (May–October). Note that the gaseous O_2 (a,b) measurements were obtained at 25, 50, 75*

521   *and 150 cm depths and the E_h conditions (c,d) were observed at 25, 50, 75 and 100 cm depths. All*

522   *observations were conducted in station 2. The data are separated between summer and winter according*

523   *to the trends presented in* Figure 5. *The green, grey, and yellow areas represent the oxic (400mV <),*

524   *suboxic (400mV > E_h > 100mV), and anoxic E_h < 100mV) conditions, respectively.*

525

4 Summary and Conclusions

527   Continuous monitoring of E_h, θ, T, and gaseous O_2 in the vadose zones of SAT infiltration ponds

528   was carried out for about 600 days. SAT operation was subjected to long and short wetting and

529   drying cycles and seasonal changes. The datasets enabled the examination of factors that control

530   the hydrological and geochemical conditions in SAT. Calibrated and validated hydrological

531   models were applied to investigate the water flow dynamics in the SAT vadose zone. E_h and

532   gaseous O_2 observations were averaged to determine seasonal changes and deduce the optimal

533   length of wetting and drying stages.

534   The examination of the measured E_h conditions illustrated a noticeable decline to markedly

535   negative values (-450mV >) during summer and to values between 0 and -50 mV during winter.

536   These E_h conditions were established following 30 hours of wetting, and no considerable

537   changes in E_h conditions were noticeable until the wetting stages ceased. A monthly statistic of

538   the E_h measurements illustrated the relationship between the size of the E_h amplitude and the

539   seasonal T changes. Furthermore, it is speculated that the limited decrease in E_h conditions

540   during winter were due to lower microbial activity. An additional support for this claim is the

541   reduction in infiltration capabilities following long wetting and drying cycles during winter, as

542   was indicated by the hydrological models. To define the optimal length of a wetting stage, the E_h

543   data were averaged and separated between the winter and summer periods. During the summer

544   period, the optimal time length of a wetting stage, according to E_h observations, is about 30

545   hours. Determining the optimal length of a wetting stage during winter is challenging.

546   Practically, there are no significant differences between E_h conditions during winter and summer

547   for the first 28 hours of wetting. Thus, the length of a wetting stage during winter should be 30

548   hours, as in the summer period.

549   The length of a drying stage, following the E_h observations, should be about 36 hours, regardless

550   of the initial values of the E_h conditions and the season. Note that during summer, a longer drying

551   time is required for the E_h conditions to attain suboxic conditions. Nevertheless, the gaseous O_2

552   observations indicated faster aeration rates during summer, which compensate for the very

553   negative E_h conditions and allow fast recovery. Following our analysis, we suggest that under the

554   tested conditions, the length of a drying stage should be 36 hours for winter and summer. Shorter

555   drying stages would affect SAT efficiency, while applying longer drying stages would reduce the

556   total hydraulic loads that can be fed to the infiltration basin.

557   Implementing in situ E_h, θ, T and gaseous O_2 sensors provided continuous high-resolution

558   observations. These datasets revealed the hydrological and biochemical dynamics in SAT as

559   imposed by seasonal and operational changes. Analysis of the E_h and O_2 measurements enabled

560   the identification of the optimal time lengths of wetting and drying stages. The results indicated

561   that there is no direct relationship between the length of a wetting stage and a drying stage. Thus,

562   the operational use of a wetting/drying ratio in SAT management should be reconsidered.

563

564   *Data availability.* The data that support the findings of this study are available from the

565   corresponding author, Tuvia Turkeltaub, upon reasonable request.

566   *Author contributions.* RM, AF and NW designed the experiments, RM provided the field data,

567   TT preformed the data analyses and prepared the paper with contribution of all authors.

568   *Competing interests.* The authors declare that they have no conflict of interest.

569   *Acknowledgments.* This work was financed within the framework of the German–Israeli Water

570   Technology Cooperation Program under Project No. WT1601/2689, by the German Federal

571   Ministry of Education and Research (BMBF), and by the Israel Ministry of Science, Technology

572   and Space (MOST).

573

References

574

575 Amy, G. and Drewes, J.: Soil aquifer treatment (SAT) as a natural and sustainable wastewater

576 reclamation/reuse technology: Fate of wastewater effluent organic Matter (EfoM) and trace

577 organic compounds, Environ. Monit. Assess., 129, 19–26, https://doi.org/10.1007/s10661-006-

578 9421-4, 2007.

579 Arye, G., Tarchitzky, J., and Chen, Y.: Treated wastewater effects on water repellency and soil

580 hydraulic properties of soil aquifer treatment infiltration basins, J. Hydrol., 397, 136–145,

581 https://doi.org/10.1016/j.jhydrol.2010.11.046, 2011.

582 Asano, T. and Cotruvo, J. A.: Groundwater recharge with reclaimed municipal wastewater:

583 Health and regulatory considerations, Water Res., 38, 1941–1951,

584 https://doi.org/10.1016/j.watres.2004.01.023, 2004.

585 Ben-Noah, I., Nitsan, I., Cohen, B., Kaplan, G., and Friedman, S. P.: Soil aeration using air

586 injection in a citrus orchard with shallow groundwater, Agric. Water Manag., 245, 106664,

587 https://doi.org/10.1016/j.agwat.2020.106664, 2021.

588 Berner, R. A.: A new geochemical classification of sedimentary environments, J. Sediment.

589 Perology, 51, 359–365, https://doi.org/https://doi.org/10.1306/212F7C7F-2B24-11D7-

590 8648000102C1865D, 1981.

591 Bohrerova, Z., Stralkova, R., Podesvova, J., Bohrer, G., and Pokorny, E.: The relationship

592 between redox potential and nitrification under different sequences of crop rotations, Soil Tillage

593 Res., 77, 25–33, https://doi.org/10.1016/j.still.2003.10.006, 2004.

594 Bouwer, H.: Artificial recharge of groundwater: Hydrogeology and engineering, Hydrogeol. J.,

595 10, 121–142, https://doi.org/10.1007/s10040-001-0182-4, 2002.

596 Brettar, I., Sanchez-Perez, J. M., and Trémolières, M.: Nitrate elimination by denitrification in

597 hardwood forest soils of the Upper Rhine floodplain - Correlation with redox potential and

598 organic matter, Hydrobiologia, 469, 11–21, https://doi.org/10.1023/A:1015527611350, 2002.

599 Christensen, T. H., Bjerg, P. L., Banwart, S. A., Jakobsen, R., Heron, G., and Albrechtsen, H. J.:

600 Characterization of redox conditions in groundwater contaminant plumes, J. Contam. Hydrol.,

601 45, 165–241, https://doi.org/10.1016/S0169-7722(00)00109-1, 2000.

602 Cook, F. J. and Knight, J. H.: Oxygen Transport to Plant Roots, Soil Sci. Soc. Am. J., 67, 20–31,

603 https://doi.org/10.2136/sssaj2003.2000, 2003.

604 Díaz-Cruz, M. S. and Barceló, D.: Trace organic chemicals contamination in ground water

605 recharge, Chemosphere, 72, 333–342, https://doi.org/10.1016/j.chemosphere.2008.02.031, 2008.

606 Dillon, P.: Future management of aquifer recharge, Hydrogeol. J., 13, 313–316,

607 https://doi.org/10.1007/s10040-004-0413-6, 2005.

608 Doerr, S. H., Shakesby, R. A., and Walsh, R. P. D.: Soil water repellency: Its causes,

609 characteristics and hydro-geomorphological significance, Earth Sci. Rev., 51, 33–65,

610 https://doi.org/10.1016/S0012-8252(00)00011-8, 2000.

611 Drewes, J. E.: Ground water replenishment with recycled water - Water quality improvements

612 during managed aquifer recharge, Ground Water, 47, 502–505, https://doi.org/10.1111/j.1745-

613 6584.2009.00587_5.x, 2009.

614 Dutta, T., Carles-Brangarí, A., Fernàndez-Garcia, D., Rubol, S., Tirado-Conde, J., and Sanchez-

615 Vila, X.: Vadose zone oxygen (O2) dynamics during drying and wetting cycles: An artificial

616 recharge laboratory experiment, J. Hydrol., 527, 151–159,

617 https://doi.org/10.1016/j.jhydrol.2015.04.048, 2015.

618 Elkayam, R., Sopliniak, A., Gasser, G., Pankratov, I., and Lev, O.: Oxidizer Demand in the

619 Unsaturated Zone of a Surface-Spreading Soil Aquifer Treatment System, Vadose Zo. J., 14,

620 vzj2015.03.0047, https://doi.org/10.2136/vzj2015.03.0047, 2015.

621 Essandoh, H. M. K., Tizaoui, C., and Mohamed, M. H. A.: Removal of dissolved organic carbon

622 and nitrogen during simulated soil aquifer treatment, Water Res., 47, 3559–3572,

623 https://doi.org/10.1016/j.watres.2013.04.013, 2013.

624 Fox, P., Aboshanp, W., and Alsamadi, B.: during Soil Aquifer Treatment, 163, 156–163, 2005.

625 Froelich, P. N., Klinkhammer, G. P., Bender, M. L., Luedtke, N. A., Heath, G. R., Cullen, D.,

626 Dauphin, P., Hammond, D., Hartman, B., and Maynard, V.: Early oxidation of organic matter in

627 pelagic sediments of the eastern equatorial Atlantic: suboxic diagenesis, Geochim. Cosmochim.

628 Acta, 43, 1075–1090, https://doi.org/10.1016/0016-7037(79)90095-4, 1979.

629   Ganot, Y., Holtzman, R., Weisbrod, N., Nitzan, I., Katz, Y., and Kurtzman, D.: Monitoring and

630   modeling infiltration-recharge dynamics of managed aquifer recharge with desalinated seawater,

631   Hydrol. Earth Syst. Sci., 21, 4479–4493, https://doi.org/10.5194/hess-21-4479-2017, 2017.

632   Goren, O., Lazar, B., Burg, A., and Gavrieli, I.: Mobilization and retardation of reduced

633   manganese in sandy aquifers: Column experiments, modeling and implications, Geochim.

634   Cosmochim. Acta, 96, 259–271, https://doi.org/10.1016/j.gca.2012.06.032, 2012.

635   Goren, O., Burg, A., Gavrieli, I., Negev, I., Guttman, J., Kraitzer, T., Kloppmann, W., and Lazar,

636   B.: Biogeochemical processes in infiltration basins and their impact on the recharging effluent,

637   the soil aquifer treatment (SAT) system of the Shafdan plant, Israel, Appl. Geochemistry, 48,

638   58–69, https://doi.org/10.1016/j.apgeochem.2014.06.017, 2014.

639   Gorski, G., Fisher, A. T., Beganskas, S., Weir, W. B., Redford, K., Schmidt, C., and Saltikov, C.:

640   Field and Laboratory Studies Linking Hydrologic, Geochemical, and Microbiological Processes

641   and Enhanced Denitrification during Infiltration for Managed Recharge, Environ. Sci. Technol.,

642   53, 9491–9501, https://doi.org/10.1021/acs.est.9b01191, 2019.

643   Grau-martínez, A., Torrentó, C., Carrey, R., Rodríguez-escales, P., Domènech, C., Ghiglieri, G.,

644   Soler, A., and Otero, N.: Feasibility of two low-cost organic substrates for inducing denitri fi

645   cation in arti fi cial recharge ponds : Batch and fl ow-through experiments, J. Contam. Hydrol.,

646   198, 48–58, https://doi.org/10.1016/j.jconhyd.2017.01.001, 2017.

647   Grau-martínez, A., Folch, A., Torrentó, C., Valhondo, C., Barba, C., Domènech, C., Soler, A.,

648   and Otero, N.: Monitoring induced denitrification during managed aquifer recharge in an

649   infiltration pond, J. hydroloy, 561, 123–135, https://doi.org/10.1016/j.jhydrol.2018.03.044, 2018.

650   Greskowiak, J., Prommer, H., Massmann, G., and Nützmann, G.: Modeling seasonal redox

651   dynamics and the corresponding fate of the pharmaceutical residue phenazone during artificial

652   recharge of groundwater, Environ. Sci. Technol., 40, 6615–6621,

653   https://doi.org/10.1021/es052506t, 2006.

654   Grinshpan, M., Furman, A., Dahlke, H. E., Raveh, E., and Weisbrod, N.: From managed aquifer

655   recharge to soil aquifer treatment on agricultural soils: Concepts and challenges, Agric. Water

656   Manag., 255, 106991, https://doi.org/10.1016/j.agwat.2021.106991, 2021.

657 Grinshpan, M., Turkeltaub, T., Furman, A., Raveh, E., and Weisbrod, N.: On the use of orchards

658 to support soil aquifer treatment systems, Agric. Water Manag., 260,

659 https://doi.org/10.1016/j.agwat.2021.107315, 2022.

660 Guswa, A. J., Celia, M. A., and Rodriguez-Iturbe, I.: Models of soil moisture dynamics in

661 ecohydrology: A comparative study, Water Resour. Res., 38, 5-1-5–15,

662 https://doi.org/10.1029/2001wr000826, 2002.

663 Hargreaves, J. A.: Photosynthetic suspended-growth systems in aquaculture, Aquac. Eng., 34,

664 344–363, https://doi.org/10.1016/j.aquaeng.2005.08.009, 2006.

665 Hinchey, E. K. and Schaffner, L. C.: An evaluation of electrode insertion techniques for

666 measurement of redox potential in estuarine sediments, Chemosphere, 59, 703–710,

667 https://doi.org/10.1016/j.chemosphere.2004.10.029, 2005.

668 Ickeson-Tal, N., Avraham, O., Sack, J., and Cikurel, H.: Water reuse in Israel – the Dan region

669 project: evaluation of water quality and reliability of plant's operation., 3, 231–237, 2003.

670 Inbar, Y.: New standards for treated wastewater reuse in Israel, in: In: Zaidi M, editor.

671 Wastewater reuse—risk assessment, decision-making and environmental security., Dordrecht,

672 The Netherlands: Springer; 2007. p. 291–6., 2007.

673 Kfir, O., Tal, A., Gross, A., and Adar, E.: The effect of reservoir operational features on recycled

674 wastewater quality, Resour. Conserv. Recycl., 68, 76–87,

675 https://doi.org/10.1016/j.resconrec.2012.08.002, 2012.

676 Kirschbaum, M. U. F.: The temperature dependence of soil organic matter decomposition, and

677 the effect of global warming on soil organic C storage, Soil Biol. Biochem., 27, 753–760,

678 https://doi.org/10.1016/0038-0717(94)00242-S, 1995.

679 Lin, C., Greenwald, D., and Banin, A.: Temperature dependence of infiltration rate during large

680 scale water recharge into soils, Soil Sci. Soc. Am. J., 67, 487–493,

681 https://doi.org/10.2136/sssaj2003.4870, 2003.

682 Lin, C., Eshel, G., Negev, I., and Banin, A.: Long-term accumulation and material balance of

683 organic matter in the soil of an effluent infiltration basin, Geoderma, 148, 35–42,

684 https://doi.org/10.1016/j.geoderma.2008.09.017, 2008.

685   Mächler, L., Peter, S., Brennwald, M. S., and Kipfer, R.: Excess air formation as a mechanism

686   for delivering oxygen to groundwater, Water Resour. Res., 49, 6847–6856,

687   https://doi.org/10.1002/wrcr.20547, 2013.

688   Massmann, G., Greskowiak, J., Dünnbier, U., Zuehlke, S., Knappe, A., and Pekdeger, A.: The

689   impact of variable temperatures on the redox conditions and the behaviour of pharmaceutical

690   residues during artificial recharge, J. Hydrol., 328, 141–156,

691   https://doi.org/10.1016/j.jhydrol.2005.12.009, 2006.

692   McMahon, P. B. and Chapelle, F. H.: Redox processes and water quality of selected principal

693   aquifer systems, Ground Water, 46, 259–271, https://doi.org/10.1111/j.1745-6584.2007.00385.x,

694   2008.

695   Miller, J. H., Ela, W. P., Lansey, K. E., Chipello, P. L., and Arnold, R. G.: Nitrogen

696   Transformations during Soil–Aquifer Treatment of Wastewater Effluent—Oxygen Effects in

697   Field Studies, J. Environ. Eng., 132, 1298–1306, https://doi.org/10.1061/(asce)0733-

698   9372(2006)132:10(1298), 2006.

699   Mizrahi, G., Furman, A., and Weisbrod, N.: Infiltration under Confined Air Conditions: Impact

700   of Inclined Soil Surface, Vadose Zo. J., 15, vzj2016.04.0034,

701   https://doi.org/10.2136/vzj2016.04.0034, 2016.

702   Morrison, C. M., Betancourt, W. Q., Quintanar, D. R., Lopez, G. U., Pepper, I. L., and Gerba, C.

703   P.: Potential indicators of virus transport and removal during soil aquifer treatment of treated

704   wastewater effluent, Water Res., 177, 115812, https://doi.org/10.1016/j.watres.2020.115812,

705   2020.

706   Ben Moshe, S., Weisbrod, N., Barquero, F., Sallwey, J., Orgad, O., and Furman, A.: On the role

707   of operational dynamics in biogeochemical efficiency of a soil aquifer treatment system, Hydrol.

708   Earth Syst. Sci., 24, 417–426, https://doi.org/10.5194/hess-24-417-2020, 2020.

709   Ben Moshe, S., Weisbrod, N., and Furman, A.: Optimization of soil aquifer treatment (SAT)

710   operation using a reactive transport model, Vadose Zo. J., 1–13,

711   https://doi.org/10.1002/vzj2.20095, 2021.

712   Nadav, I., Arye, G., Tarchitzky, J., and Chen, Y.: Enhanced infiltration regime for treated-

wastewater purification in soil aquifer treatment (SAT), J. Hydrol., 420–421, 275–283,

https://doi.org/10.1016/j.jhydrol.2011.12.013, 2012a.

Nadav, I., Tarchitzky, J., and Chen, Y.: Soil cultivation for enhanced wastewater infiltration in

soil aquifer treatment (SAT), J. Hydrol., 470–471, 75–81,

https://doi.org/10.1016/j.jhydrol.2012.08.013, 2012b.

Negev, I., Shechter, T., Shtrasler, L., Rozenbach, H., and Livne, A.: The effect of soil tillage

equipment on the recharge capacity of infiltration ponds, 12, 1–11,

https://doi.org/10.3390/w12020541, 2020.

Nimmo, J. R., Schmidt, K. M., Perkins, K. S., and Stock, J. D.: Rapid Measurement of Field-

Saturated Hydraulic Conductivity for Areal Characterization, Vadose Zo. J., 8, 142–149,

https://doi.org/10.2136/vzj2007.0159, 2009.

Oren, O., Gavrieli, I., Burg, A., Guttman, J., and Lazar, B.: Manganese mobilization and

enrichment during soil aquifer treatment (SAT) of effluents, the Dan Region Sewage

Reclamation Project (Shafdan), Israel, Environ. Sci. Technol., 41, 766–772,

https://doi.org/10.1021/es060576+, 2007.

Quanrud, D. M., Arnold, R. G., Wilson, L. G., Gordon, H. J., Graham, D. W., and Amy, G. L.:

Fate of Organics during Column Studies of Soil Aquifer Treatment, J. Environ. Eng., 122, 314–

321, https://doi.org/10.1061/(asce)0733-9372(1996)122:4(314), 1996.

Quanrud, D. M., Hafer, J., Karpiscak, M. M., Zhang, J., Lansey, K. E., and Arnold, R. G.: Fate

of organics during soil-aquifer treatment: Sustainability of removals in the field, Water Res., 37,

3401–3411, https://doi.org/10.1016/S0043-1354(02)00489-X, 2003.

Reedy, K. R., D'Angelo, E. M., and Harris, W. G.: Biochemistry of wetlands, in: Handbook of

Soil Science, edited by: Summer, M. E., 89–119, 2000.

Rezanezhad, F., Couture, R. M., Kovac, R., O'Connell, D., and Van Cappellen, P.: Water table

fluctuations and soil biogeochemistry: An experimental approach using an automated soil

column system, J. Hydrol., 509, 245–256, https://doi.org/10.1016/j.jhydrol.2013.11.036, 2014.

Ritter, A. and Muñoz-Carpena, R.: Performance evaluation of hydrological models: Statistical

significance for reducing subjectivity in goodness-of-fit assessments, J. Hydrol., 480, 33–45,

741 https://doi.org/10.1016/j.jhydrol.2012.12.004, 2013.

742 Rodríguez-Escales, P., Barba, C., Sanchez-Vila, X., Jacques, D., and Folch, A.: Coupling Flow,

743 Heat, and Reactive Transport Modeling to Reproduce in Situ Redox Potential Evolution:

744 Application to an Infiltration Pond, Environ. Sci. Technol., 54, 12092–12101,

745 https://doi.org/10.1021/acs.est.0c03056, 2020.

746 Sallwey, J., Jurado, A., Barquero, F., and Fahl, J.: Enhanced removal of contaminants of

747 emerging concern through hydraulic adjustments in soil aquifer treatment, 12,

748 https://doi.org/10.3390/w12092627, 2020.

749 Sattar, A. M. A.: Prediction of Organic Micropollutant Removal in Soil Aquifer Treatment

750 System Using GEP, J. Hydrol. Eng., 21, 04016027, https://doi.org/10.1061/(asce)he.1943-

751 5584.0001372, 2016.

752 Schmidt, C. M., Fisher, A. T., Racz, A. J., Lockwood, B. S., and Huertos, M. L.: Linking

753 denitrification and infiltration rates during managed groundwater recharge, Environ. Sci.

754 Technol., 45, 9634–9640, https://doi.org/10.1021/es2023626, 2011.

755 Sharma, S. K. and Kennedy, M. D.: Soil aquifer treatment for wastewater treatment and reuse,

756 Int. Biodeterior. Biodegrad., 119, 671–677, https://doi.org/10.1016/j.ibiod.2016.09.013, 2017.

757 Shenker, M., Seitelbach, S., Brand, S., Haim, A., and Litaor, M. I.: Redox reactions and

758 phosphorus release in re-flooded soils of an altered wetland, Eur. J. Soil Sci., 56, 515–525,

759 https://doi.org/10.1111/j.1365-2389.2004.00692.x, 2005.

760 Silver, M., Knöller, K., Schlögl, J., Kübeck, C., and Schüth, C.: Nitrogen cycling and origin of

761 ammonium during infiltration of treated wastewater for managed aquifer recharge, Appl.

762 Geochemistry, 97, 71–80, https://doi.org/10.1016/j.apgeochem.2018.08.003, 2018.

763 Skopp, J., Jawson, M. D., and Doran, J. W.: Steady-State Aerobic Microbial Activity as a

764 Function of Soil Water Content, Soil Sci. Soc. Am. J., 54, 1619–1625,

765 https://doi.org/10.2136/sssaj1990.03615995005400060018x, 1990.

766 Sopilniak, A., Elkayam, R., and Lev, O.: Nitrification in a soil-aquifer treatment system:

767 Comparison of potential nitrification and concentration profiles in the vadose zone, Environ. Sci.

768 Process. Impacts, 19, 1571–1582, https://doi.org/10.1039/c7em00402h, 2017.

769 Sopilniak, A., Elkayam, R., Rossin, A. V., and Lev, O.: Emerging organic pollutants in the

770 vadose zone of a soil aquifer treatment system: Pore water extraction using positive

771 displacement, Chemosphere, 190, 383–392, https://doi.org/10.1016/j.chemosphere.2017.10.010,

772 2018.

773 Stumm, W., & Morgan, J. J.: Aquatic chemistry (3rd ed.), Wiley, 1996.

774 Tsangaratos, P., Kallioras, A., Pizpikis, T., Vasileiou, E., Ilia, I., and Pliakas, F.: Multi-criteria

775 Decision Support System (DSS) for optimal locations of Soil Aquifer Treatment (SAT) facilities,

776 Sci. Total Environ., 603–604, 472–486, https://doi.org/10.1016/j.scitotenv.2017.05.238, 2017.

777 Tufenkji, N., Redman, J. A., and Elimelech, M.: Interpreting deposition patterns of microbial

778 particles in laboratory-scale column experiments, Environ. Sci. Technol., 37, 616–623,

779 https://doi.org/10.1021/es025871i, 2003.

780 Wallace, C. D., Sawyer, A. H., and Barnes, R. T.: Spectral analysis of continuous redox data

781 reveals geochemical dynamics near the stream–aquifer interface, Hydrol. Process., 33, 405–413,

782 https://doi.org/10.1002/hyp.13335, 2019.

783 Wallis, M. G. and Horne, D. J.: Soil water repellency, in: Advances in Soil Science, 265–267,

784 1992.

785

786

787

788

789